Atmospheric Environment 199 (2019) 380–390

Contents lists available at ScienceDirect

Atmospheric Environment

journal homepage: www.elsevier.com/locate/atmosenv

Formation of atmospheric molecular clusters consisting of methanesulfonic acid and sulfuric acid: Insights from flow tube experiments and cluster dynamics simulations

Hui Wen[a], Chun-Yu Wang[a], Zhong-Quan Wang[a], Xiao-Fei Hou[a], Ya-Juan Han[a], Yi-Rong Liu[b], Shuai Jiang[b], Teng Huang[a], Wei Huang[a,b,c,*]

[a] Laboratory of Atmospheric Physico-Chemistry, Anhui Institute of Optics & Fine Mechanics, Chinese Academy of Sciences, Hefei, Anhui, 230031, China
[b] School of Information Science and Technology, University of Science and Technology of China, Hefei, Anhui, 230026, China
[c] Center for Excellence in Urban Atmospheric Environment, Institute of Urban Environment, Chinese Academy of Sciences, Xiamen, Fujian, 361021, China

ARTICLE INFO

Keywords:
Methanesulfonic acid
Flow tube reactor
Cluster dynamics model
APi-TOF-MS
Particle formation rates

ABSTRACT

In coastal regions and ocean areas, methanesulfonic acid (MSA; CH_3SO_3H) is present in considerable concentrations in the gas-phase and aerosols. It has been shown that MSA could contribute to growth and possibly form initial molecular cluster, which may lead to aerosol formation. However, quantitative concentrations and thermodynamic properties of MSA and sulfuric acid (SA; H_2SO_4) in the presence of water (W; H_2O) remain largely uncertain. In this study, flow tube reactor was used to investigate the effects of each reactant on new particle formation (NPF) in a multi-component system consisting of MSA, SA, and W. Particles were measured for different combinations of reactants. It showed that a different order for reactant addition led to different experimental results, where the added MSA vapor to the SA-W binary system presented an obvious bimodal structure, for ternary system with SA added to the MSA-W, the similar bimodal phenomenon was not observed. The composition of clusters in the air flow was further analyzed by the commercial Atmospheric Pressure Interface Time-of-Flight Mass Spectrometer (APi-TOF-MS, Tofwerk AG), which is equipped with a homemade chemical ionization (CI) source, mass peaks corresponding to clusters that contain smaller MSA or SA molecules were clearly observed, indicating that these clusters are exist and stable. In addition, quantum chemistry calculation-based evaporation rate values were applied in a cluster dynamics model to yield formation rates of $2.6 \times 10^2\,cm^{-3}\,s^{-1}$ and cluster concentrations under different simulation conditions. This study could provide some insight into how acids interact in the atmosphere.

1. Introduction

New particle formation (NPF) in the atmosphere by gas-phase species nucleation and subsequent condensation growth is an important secondary conversion process (Kulmala et al., 2004; Zhang et al., 2012). The newly formed particles can grow to the size that they can act as cloud condensation nuclei (CCN) and in this way affect cloud and climate-relevant properties (Kerminen et al., 2005; Spracklen et al., 2008; Farmer et al., 2015). Thus, the species and mechanisms involved in NPF event must be fully understood to qualitatively or quantitatively predict impacts on atmospheric visibility, climate, and human health (Poschl, 2005; Heal et al., 2012; Zhang et al., 2012). NPF have often been observed to be related to sulfuric acid (SA; H_2SO_4) (Weber et al., 1996, 1997, 2001; Arstila et al., 1998; Noppel et al., 2002; Hanson and Lovejoy, 2006; Kuang et al., 2008; Sipila et al., 2010; Chen et al., 2012; Almeida et al., 2013), the homogeneous nucleation of SA and water (W; H_2O) has been long considered as the main source of NPF in the atmosphere. However, increasing evidence indicates that the SA-W binary nucleation is not sufficient to explain the nucleation rates measured in an actual atmospheric environment (O'Dowd et al., 1999; Aalto et al., 2001). Therefore, other substances, which are involved in nucleation phenomena, have been proposed (Kulmala and Kerminen, 2008; Kuang et al., 2010; Paasonen et al., 2010).

Atmospheric MSA is the simplest organic sulfate and is a well-known oxidation product of dimethyl sulfide (Vandergheynst et al., 1998; Rosenfeld et al., 2001; Meinardi et al., 2003; Barnes et al., 2006). In ocean areas and relatively clean coastal regions, overall median concentration for SA and MSA in marine background air was 1.5×10^6

* Corresponding author. School of Information Science and Technology, University of Science and Technology of China, Hefei, Anhui, 230026, China.
E-mail address: huangwei6@ustc.edu.cn (W. Huang).

https://doi.org/10.1016/j.atmosenv.2018.11.043
Received 16 August 2018; Received in revised form 15 November 2018; Accepted 17 November 2018
Available online 20 November 2018
1352-2310/

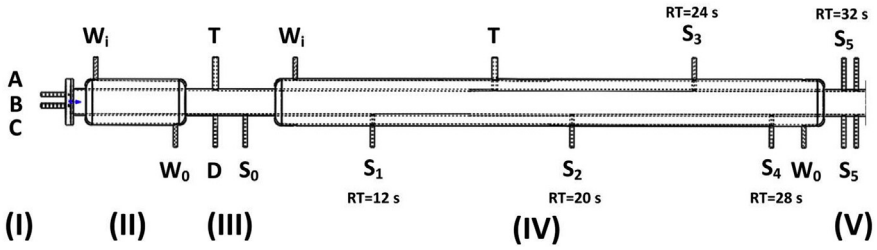

Fig. 1. . Schematic of the laminar flow tube reactor. The reactor is roughly divided into five sections: (I): reactants entered region, (II) mixing region, (III) transition region, (IV) nucleation and growth region, and (V) synchronous detection region. The letters A, B, C, and D marked in the figure represent the inlets of each reactant; W_i and W_o, the inlet and the outlet of the circulator bath for temperature control, respectively; T is a temperature and humidity detection port, and S_0-S_5 represents several sample ports along the tube, corresponding residence time (RT) of each sample port are also marked.

molecules cm^{-3} and 1.2×10^6 molecules cm^{-3}, respectively (Berresheim et al., 2002). Atmospheric concentrations of gaseous MSA range from 10^5 to 10^7 molecules cm^{-3}, which is approximately 10–100% of SA (Berresheim et al., 1993, 2002; Mauldin et al., 1999, 2003). Recently, Dall'Osto et al. (Dall'Osto et al., 2012) found that the MSA concentration decreased during marine particle formation events, suggesting that MSA may contribute to growth and possibly form initial molecular clusters, which may lead to aerosol formation (Kreidenweis et al., 1989; Wyslouzil et al., 1991a,b; Dawson et al., 2012; Bork et al., 2014b; Ezell et al., 2014; Chen et al., 2015, 2016).

Okuyama and coworkers (Wyslouzil et al., 1991a,b) have systematically studied the temperature dependence of MSA–W binary nucleation using a continuous flow mixing–type device and found that under-saturated MSA vapor in the presence of moderate relative humidity (RH) (less than 60%) can generate observed aerosol concentrations up to approximately $10^5\,cm^{-3}$. Since then, some theoretical and laboratory studies attempted to explain these findings and concluded when MSA enters the aerosol particle (Ball et al., 1999; Korhonen et al., 1999; Kurten et al., 2008; Erupe et al., 2011; Kirkby et al., 2011; Dawson et al., 2012; Yu et al., 2012; Zollner et al., 2012; Almeida et al., 2013; Ezell et al., 2014; Chen et al., 2015, 2016; Glasoe et al., 2015). In particular, the Finlayson-Pitts group conducted extensive works (Ezell et al., 2010, 2014; Zheng et al., 2010; Dawson et al., 2012, 2014; Nishino et al., 2014; Chen et al., 2015, 2016) to study the relationship between RH and precursor concentrations from the reactions of MSA with ammonia/amines using a slow aerosol flow system. They demonstrated that MSA and amines can form particles, and W plays a major role. In addition, different amines showed different dependencies on water vapor and precursor concentrations in a complex manner. Recently, it has been predicted that when the MSA and SA are present in equal amounts, the particles formed by SA and amines increase by 15–300% in the temperature range (i.e., from 258 K to 298 K) (Bork et al., 2014b). Other studies (Bzdek et al., 2011; Dawson et al., 2012) found that nitrogenous bases and W enhance MSA-based aerosol formation, and amines are more effective than ammonia when combining flow tube experiments and theoretical calculations. For the clusters containing up to two acids and one DMA molecule, Dall'Osto et al. (Dall'Osto et al., 2012) used theoretical calculations to support the hypothesis that MSA, SA, and DMA could coexist in freshly formed molecular clusters.

Although it is known that acid − base reactions play a major role in NPF in the air, it should be recognized that other composite patterns are also very important (Zhang et al., 2004; Donahue et al., 2013; Schobesberger et al., 2013; Bianchi et al., 2014, 2016; Ehn et al., 2014; Riccobono et al., 2014; Jokinen et al., 2015; Troestl et al., 2016). The combination of two acids in the presence of W molecules may also play a role. Therefore, composite patterns are needed to assess the treatment of this complex array in laboratory species and atmospheric models.

Earlier studies often used simplified classical nucleation theory (CNT) to forecast or reproduce the formation rate of particles for various mixtures of SA, MSA and W, and generally found that MSA is less important (Wyslouzil et al., 1991a; Vandingenen and Raes, 1993; Napari et al., 2002). These studies have prompted a classical nucleation theory based on the assessment of MSA contributions to aerosol formation or growth. However, there are still some inevitable limitations.

In this study, we target the enhancing effect of MSA on SA-W cluster formations through a series of experimental and theoretical studies to investigate particle formation from reaction of MSA with SA and W. The formation rate of detectable particles from reactions of MSA with SA and W, as well as the capabilities of MSA to bind to small and electrically neutral SA clusters are examined by theoretical calculations. This study could provide some insight into how acids interact in the atmosphere.

2. Methodology

2.1. Experimental section

The glass laminar flow tube reactor (Fig. 1) was used to study the formation and growth of particles at varied experimental conditions (i.e., humidities, temperatures, or reactant concentrations). The main part of the flow tube reactor is 5 cm in diameter and 180 cm in length, and is water jacketed for temperature-control. A total flow rate of 6 slpm of carrier gas was used, which had four inlets: A, B, C, and D. The source of gas in this study was dry compressed zero air from a purge air generator. Relative humidity (RH) was tuned by passing partially dry zero air through a bubbler filled with ultrapure water. Before the introduction of gas phase reactant to initiate the formation and growth of particles, a mixture of MSA/SA flow and zero air was introduced through the inlet (A) at a flow rate of 1 slpm for 1–2 days to passivate the inlet and flow tube, as well as minimize wall losses of SA or MSA. Particle formation and growth was measured at 27 ± 1 °C by adjusting the circulating water temperature. The temperature in the flow tube reactor was measured by a PT100 probe.

The dry zero air was divided into four gas paths that were connected to four inlets accordingly. One of them passed over the SA liquid, which was contained in a saturator at 40 ± 1 °C (to quantify the SA concentration) and was controlled by circulating water, to create a gas-phase SA. The MSA standard was produced by introducing a stable flow of the second zero air path through a permeation tube (VICI AG International) containing MSA, which was held at 100 °C to ensure a constant rate of permeation (permeation rate is 38 ± 50% ng/min at 100 °C, given by the supplier). The third gas line passed through ultrapure water in a bubbler to produce a hydration environment in the flow tube reactor. The last zero air flow was directly introduced into the flow tube to create a total flow to 6 slpm. SA concentrations and humidity levels were tuned by varying the flow rate; the concentration of MSA was tuned by introducing measured fractions of the flow from the permeation tube into the flow tube reactor. The ultrapure water in bubbler was held a few drops of 97% sulfuric acid to remove or minimize the possible existence contamination (i.e., amines or ammonia vapors) that may come in with the carrier gas or upon refilling with ultrapure water. The flow regime of the flow tube reactor was fully developed laminar.

SA concentration was calculated by a mass balance. The mass balance calculation provides a concentration of SA that directly comes out of the saturator and does not include any losses at any part of the tube

walls. Here, the calculated concentration of SA can represent upper concentration in the flow tube. Both SA and MSA are viscous compounds, so there might be wall losses in the flow tube inlets and even the flow tube reactor itself after thoroughly conditioning. In our study, the wall loss of SA in the flow reactor is estimated to be a diffusion controlled first-order rate process (Brus et al., 2017). The atmospheric and flow tube background experiment and self-nucleation of each separate component (i.e., MSA alone, SA alone, and W alone) experiment are also carried out to show that the binary or ternary system particle formation observed was a meaningful observation.

Particle size distributions were measured using a scanning mobility particle sizer (SMPS, Model 3938; TSI) that consists of an electrostatic classifier (Model 3082; TSI), a nano-differential mobility analyzer (Model 3085; TSI), and a butanol-based condensation particle counter (Model 3776; TSI). During the experiment, the sheath flow was set to 13 L/min and the aerosol flow set to 1.30 L/min. The manufacturer specified that the d50 cut-off value of the SMPS based on sucrose particles is approximately 2.5 nm. Although SMPS can detect some particles < 2.5 nm, depending on the size and composition (Kangasluoma et al., 2014), this part of the data has high uncertainty and therefore was excluded from quantitative analysis. The geometric mean mobility diameter (GMD) determined by the SMPS was reported as the particle diameters.

Subsequently, the flow tube was connected to a commercial Atmospheric Pressure Interface Time-of-Flight Mass Spectrometer (APi-TOF-MS, Tofwerk AG) through a sampling tube. This apparatus has high resolution, accuracy, and sensitivity. It can sample naturally charged ions directly from the atmosphere without any electronic or chemical manipulation, and can also be coupled to ionization methods to assist in the detection of the preferred ions (Junninen et al., 2010). To study the composition of the mixing clusters, the desired anions formed by a homemade nitrate chemical ionization (CI) source (Eisele and Tanner, 1993; Zheng et al., 2015) were guided by two quadruple ion guides and ion lens stacks, and detected using an MCP detector. The reagent ion, $NO_3^-(HNO_3)_n$ (n = 1–2), was generated by introducing traces of HNO_3 in a temperature-regulated bottle into a flow of pure N_2. Detailed descriptions of the apparatus were given elsewhere (Junninen et al., 2010).

2.2. Theoretical section

2.2.1. Electronic structure calculations

Basin-hopping (BH) algorithm with metropolis sampling and local optimization techniques has been successfully used to explore the structure of nanoclusters, especially for the structure of atomic clusters (Wen et al., 2013, 2014; Xu et al., 2013; Yan et al., 2013). Subsequently, the new “compressed sampling” technique combined with the Basin-Hopping has been employed to searching the structures; a detailed description of this method was given elsewhere (Liu et al., 2014). We have shown that the new technique was suitable for searching the structure of molecular clusters (Wen et al., 2016), and can also be applied when studying atmospheric clusters (Peng et al., 2016; Chen et al., 2017).

We searched the energy minimum structure of the xMSA-ySA-zW (x = 0-3, y = 0-3, and z = 0-3) clusters using the improved BH method coupled with density functional theory (DFT). To generate isomer populations in the original BH search, the gradient-corrected Perdew-Burke-Ernzerhof (PBE) exchange correlation functional (Perdew et al., 1996a) and double numerical polarized (DNP) basis set with effective core potentials (ECPs), were used in the $DMol^3$ code (Delley, 1990).

Plenty of structures were sampled for each size clusters, especially for the larger clusters. The isomers for each cluster were ranked according to their relative energies so as to be further optimized at high levels. The selected low-lying isomers in each case were optimized using the exchange component from Perdew and Wang’s 1991 (PW91) functional (Perdew et al., 1996b), with the 6-311 + + G (3df, 3pd) basis set (Raghavachari and Trucks, 1989), which was employed in the Gaussian 09 package (Frisch et al., 2009). The PW91 functional was selected for core optimization and to use as the frequency calculation method because it has shown good performance for a large number of atmospheric relevant clusters having common organic acids, including prediction of structural characteristics, thermodynamic parameters, and satisfactory similarities compared with the experimental results (Nadykto and Yu, 2007; Nadykto et al., 2015; Xu et al., 2010; Xu and Zhang, 2012; Bork et al., 2014a; Elm et al., 2017).

Single point energy (SP) calculations were completed at a high level of theory, DF-LMP2-F12, with a PVTZ basis set. The DF-LMP2-F12 calculations were implemented with the Molpro 2010.1 (Werner et al., 2010, 2012). Because there can be significant differences in quantitative energy values calculated at different quantum chemical levels of theory, the electronic energies of the smallest clusters consisting of one SA and one MSA molecule were also computed under the CCSD(T)-F12a levels (with Molpro 2010.1) using the VDZ-F12 basis set to assess uncertainties related to initial clustering; we found that values obtained by the DF-LMP2-F12/PVTZ were consistent with those obtained under the CCSD(T)-F12a/VDZ-F12 level of theory. The energy values in the current paper were all calculated under the DF-LMP2-F12/PVTZ level.

2.2.2. Atmospheric cluster dynamics code modeling simulations

Data from the quantum chemistry calculations were implemented in a dynamics model to simulate the kinetics of molecular cluster populations, as well as to study steady-state concentrations, formation pathways, and formation rates of the clusters. The details of the dynamic cluster model were presented in a previous study (McGrath et al., 2012). Briefly, the model generates and solves cluster birth–death equations; that is, time derived from the cluster concentrations to obtain the time development of the concentrations for all clusters included in the simulation. The time derivatives include all possible collisions and evaporation processes between simulated clusters and molecules, as well as possible external sources and sink terms. The collision rate constants were calculated from the kinetic gas theory, which assumes that spherical clusters with radii calculated with the molecular masses (18.02, 98.08, and 96.11 g mol^{-1} for W, SA, and MSA, respectively) and liquid densities (997, 1830, and 1481 kg m^{-3} for W, SA, and MSA, respectively; which were mostly determined at 20–25 °C) from the pure compounds assume ideal mixing. The evaporation rate constants were calculated from the free energy of formation of the clusters according to a detailed balance concept (Henschel et al., 2016).

The Atmospheric Cluster Dynamics Code (ACDC) simulations were consistent with the experimental conditions, mainly running at 298.15 K. A constant coagulation sink coefficient (sink term) was set to 2.6×10^{-3} s^{-1}, a typical sink for boreal forest environments, and also the median condensation sink coefficient of sulfuric acid vapor on pre-existing aerosol particles (Dal Maso et al., 2007). The SA concentration was set from 4.0×10^8 to 7.0×10^9 cm^{-3}, a range relevant to the flow tube experiment. MSA concentrations were set between 1.6 ppb ($\sim 4.0 \times 10^{10}$ cm^{-3}) and 2.4 ppb ($\sim 5.9 \times 10^{10}$ cm^{-3}). The hydration effect was also considered, and relative humidities were set to 0%, 10%, 20%, 30%, 40%, and 60%, accordingly.

3. Results and discussion

3.1. Flow tube experiment

A flow tube reactor was used to study the effect of each reactant on NPF in a multi-component system consisting of MSA, SA, and W. Particles were measured for different combinations of the reactants, typical particle size distribution data for the SA-W/MSA-W binary nucleation, as well as the ternary system for different addition orders, as shown in Fig. 2 (for a relative humidity of 30 ± 1% and residence time of 28 s corresponding to sample port S_4 in Fig. 1).

It should be noted that the SA concentration used here is about

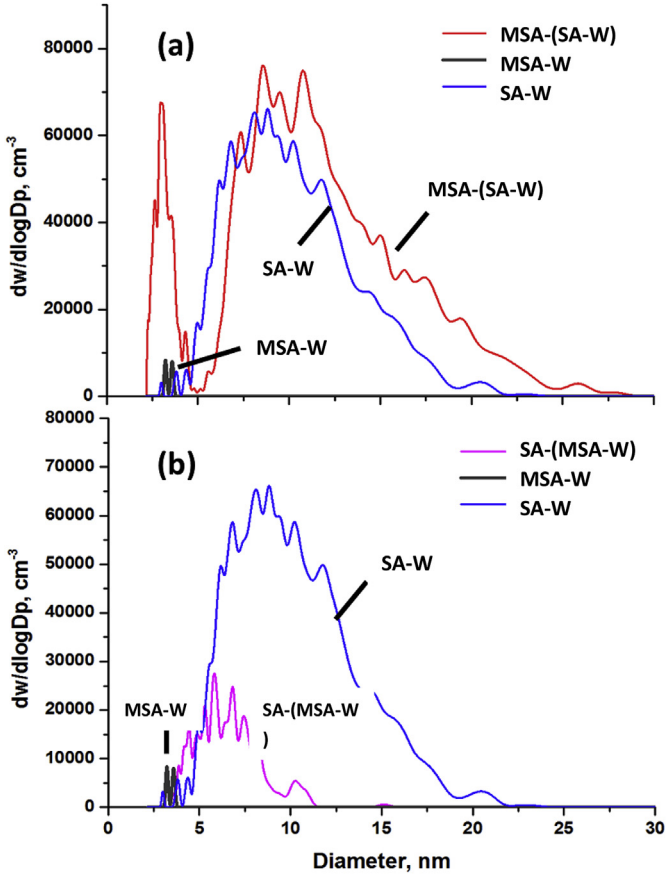

Fig. 2. Particle size distribution measured by scanning mobility particle sizer (SMPS) for the ternary system with different adding orders: (a) MSA acts on the SA-W binary system (red line), and (b) SA acts on the MSA-W binary system (purple line). Binary systems MSA-W (dark gray line) and SA-W (blue line) are also presented for comparison in each plot. Measurements were performed at an SA concentration of $4.0 \times 10^9 \pm 35\%$ molecule cm^{-3}, an MSA concentration of $4.0 \times 10^{10} \pm 50\%$ molecule cm^{-3}, an RH of 30 ± 1%, a temperature of 27 ± 1 °C, and a residence time of 28 s.

$4.0 \times 10^9 \pm 35\%$ molecule cm^{-3}, however, the MSA concentration is $4.0 \times 10^{10} \pm 50\%$ molecule cm^{-3}, which is an order of magnitude higher than the SA concentration, and inconsistent with the real situation in the atmosphere. There are two main reasons: 1) the current concentration of MSA was the minimum concentration we can get (permeation rate of MSA is 38 ng/min at 100 °C, given by the supplier), and 2) it can be studied whether excess MSA has an effect on the SA-W binary nucleation. Although the concentration of the acids used in the experiment was excessive compared to the real atmosphere, it can also reflect some essential problems over oceans and in coastal regions. In Fig. 2, the binary systems for MSA-W (black) and SA-W (blue) are presented for comparison. There were almost no particles observed from the MSA-W binary species, which is consistent with earlier studies (Kreidenweis et al., 1989; Wyslouzil et al., 1991a,b), and specially consistent with the results obtained at MSA concentration of 1.8 ppb ($\sim 4.4 \times 10^{10}$ molecule cm^{-3}) and RH of 50%, conducted by Finlayson-Pitts group (Chen et al., 2015), suggesting that background contamination is negligible. It may be necessary to use higher MSA concentrations than those used in this study to form detectable particles from MSA-W system. The number concentration of particles formed from the SA-W binary was observed at almost $2.2 \times 10^4 \pm 35\%$ per cm^3, and the geometric mean mobility diameter was measured as 8.8 ± 30% nm, which is statistically consistent with the values in previous studies (~7.7 nm) measured at an SA concentration of 1.0×10^{10} cm^{-3}, RH = 27%, T = 29 ± 2 °C, and exposure time of 20 s (Zollner et al., 2012).

In Fig. 2(a), the red curve labeled MSA-(SA-W) shows the effect of addition MSA to the SA-W binary species. Once the particles were formed from SA-W, the MSA vapor was added from the inlet D in Fig. 1, the total particle number concentration increased to $4.0 \times 10^4 \pm 40\%$ per cm^3 from about $2.2 \times 10^4 \pm 35\%$ per cm^3. It shows a bimodal distribution where the first peak may attribute to the MSA-W for the smaller particles and the second peak is due to the SA-W for the larger particles. Compared to the MSA-W binary system, the position of the first peak is slightly shifts to the relatively smaller region, and is sharp and narrow, which may means that many particles were formed. The second peak is consistent with the SA-W binary system, but the peak position shifts to the relatively larger region, which results in a larger particle diameter of 9.3 ± 35% nm. During the experiment, the MSA concentration is an order of magnitude higher than the SA concentration, this bimodal peak structure phenomenon may also indicate that excess MSA could not only participate in the peak diameter shift and the broadening, but could also be forming new particles with W.

In contrast, for Fig. 2(b), a similar bimodal phenomenon was not observed with added SA vapor to the MSA-W binary system. The particle number concentrations increased to $6.2 \times 10^3 \pm 35\%$ per cm^3 from relatively fewer particles ($1.3 \times 10^2 \pm 50\%$ per cm^3), and the particle diameter also increased rapidly to 6.8 ± 35% nm from 3 ± 50% nm, compared to the MSA-W binary system. The reason for the absence of a bimodal structure may be that the acidity of SA (i.e., pK_a of −2.0) is stronger than MSA (i.e., pK_a of −1.9) (Arquero et al., 2017) and SA may substitution into MSA-W system, and further affect the experimental results, whereas the acidity of MSA is weaker and could not affect the relatively stronger SA-W binary system.

It has been reported that MSA-W does not form particles as efficiently as SA-W, it may not be important in the atmosphere (Kreidenweis et al., 1989; Wyslouzil et al., 1991a,b), however, the Finlayson-Pitts group showed that the addition of amines to MSA-W would change this conclusion rather dramatically (Ezell et al., 2010; Dawson et al., 2012). In the current study, although the particle number concentration and the diameter of the SA-(MSA-W) ternary nucleation system were smaller when compared to the SA-W system, the particle number concentration of SA-W was enhanced by approximately 1.7 times with the addition of 4.0×10^{10} molecule cm^{-3} of MSA, indicating that the role of MSA cannot be ignored in the atmosphere, especially for the coastal area with higher levels of MSA. Compared with the MSA-W binary system, both the ternary systems MSA-(SA-W) or SA-(MSA-W) have significant increase in particle number concentration and particle diameter. Negative influences were found for both the number concentrations and diameters from the SA-(MSA-W) ternary system ($6.2 \times 10^3 \pm 35\%$ per cm^3 and 6.9 ± 35% nm) to the SA-W system ($2.2 \times 10^4 \pm 35\%$ per cm^3 and 8.8 ± 30% nm); detailed values are presented in Table S1 in the supporting information (SI). Other experimental studies, such as the particle number concentrations and the diameters of different systems as a function of residence time, are also present in Figs. S1 and S2 in the SI.

Formation Rates of detectable particles (J_{exp}) were estimated by $J_{exp} = N_{exp}/t$ (in units of cm^{-3} s^{-1}) (Brus et al., 2010), where N_{exp} is the maximum number concentration measured along the flow tube (i.e., the average over the duration of the experiment), and t is the corresponding reaction time of the maximum number concentration. In general, nucleation studies have limited accuracy for the evaluations of some quantities, such as nucleation times and SA losses. Information of air flows, temperatures, reaction times, and wall losses obtained from computational fluid dynamics may help to compensate for this lack (Panta et al., 2012; Zollner et al., 2012; Glasoe et al., 2015). Recent computational fluid dynamic simulations (Panta et al., 2012) present details of the nucleation time and reactant distribution, and show that the above equation can yield reasonable results under various conditions.

In this study, experimental determined J_{exp} were estimated by

taking the particle number concentrations at the measurement time (28 s) and dividing by 28 s; this resulted in rates of formation of $J_{exp(MSA\text{-}(SA\text{-}W))} = 1.06 \times 10^3 \pm 40\%$ cm^{-3} s^{-1} and $J_{exp(SA\text{-}(MSA\text{-}W))} = 1.89 \times 10^2 \pm 36\%$ cm^{-3} s^{-1}, respectively. For the two ternary systems, the formation rate of the MSA-(SA-W) was higher than the SA-(MSA-W), this is reasonable since the nucleation rate of SA-W binary system is larger than that of MSA-W. Here, the formation rates were calculated from the equation ($J_{exp} = N_{exp}/t$), which assumes that: 1) the particle formation rate does not take into account particles smaller than 2.5 nm, because this part of the data has greater uncertainty; 2) the coagulation losses of nucleated clusters to walls/larger particles have been neglected. The growth of the critical clusters to the minimum detected size may be disturbed by the flow tube wall losses. If this loss is significant, the values determined by the N_{exp}/t may not be simply related to the true nucleation rate; 3) the residence time used here is the actual nucleation and new particle formation reaction time, and is roughly calculated based on the volumetric flow rate and volume of flow reactor, which is a relatively poor estimate of reaction time. However, this formula can be used to roughly comparisons between experiment results, since the flow regime is laminar, error or uncertainty in reaction time is not that important when comparing the formation rates J_{exp} between experiments in the flow reactor (with same residence times).

3.2. Flow tube – mass spectrometer study

A flow tube combined with a particle sizer is an effective way to study NPF event by both number concentration and diameter from macro perspective. However, comparing particle counter measurements to predictions of cluster stabilities is not straight-forward; counters mainly detect clusters larger than what can be studied with quantum chemistry and do not provide direct information on the cluster composition. Instead, high-resolution mass spectrometers can be used to study the elemental composition of electrically charged clusters at the single molecules level, and the same method can be used for electrically neutral clusters by combining a chemical ionization unit with a mass spectrometer (CIMS).

Despite recent advances in theory and instrumentation, the chemical elementary composition of molecular clusters that form thermally stable aerosol particles remains uncertain. To get further insight into the particles forming in the flow tube reactor, as well as the cluster stability from a microscopic perspective, we performed measurements using the commercial apparatus APi-TOF-MS. A homemade CI source was seamlessly connected to the inlet of the APi-TOF-MS. The reagent ion, $NO_3^-\cdot(HNO_3)_n$ (n = 1–2), was generated by introducing traces of HNO_3 in a temperature-regulated bottle into a flow of approximately 2 slpm of pure N_2. The mixture gas composed of HNO_3 vapor and pure N_2 then passed through the CI source, causing clusters that were more acidic than the $NO_3^-\cdot(HNO_3)_n$ ions. This experimental method resulted in significantly higher concentrations than those commonly found in ambient air; therefore, the improved signal-to-noise ratio enables us to study the reactions between gas-phase species in ambient air and SA/MSA that contain clusters.

The sample port of the flow tube was set as close to the interface of the CI-APi-TOF-MS as possible and was connected by a sample tube. The mixture that formed in the flow tube was ionized by the CI source; the negatively charged ions or cluster ions were then guided into the CI-APi-TOF-MS. A small fraction of flow (approximately 200 sccm) was introduced through a 150 μm diameter hole into the vacuum chamber, and the data were analyzed using a Matlab-based program tool. Signals for different clusters differed greatly. The selected separated mass spectra of several clusters are presented in Fig. 3.

To get a better view for comparison, the background noise (red curve) was also detected. Although the backgrounds were omnipresent, flow tube signals were much stronger, indicating that the marked small clusters are real and stable. As shown in Fig. 3, the size of the measured clusters is relatively small, especially for bare acid (a) and small binary clusters (b, c, and d). In spite of the weak signals observed for the smallest ternary cluster (e) and the negatively charged clusters containing 2MSA and 2SA (f), this method proved that the mentioned clusters exist and were still stable.

While measurements of clusters containing larger sizes of SA or MSA in the core ions were very difficult and not observed with our APi-TOF-MS; this may be due to the clusters were present at low concentrations, and the clusters may be lost from the core ions during ionization, particularly for ions containing larger size molecules. Nevertheless, the main trend in the flow tube may still be reflected, especially when compared with the atmospheric background results. The mass spectrometer technique can, however, affect the composition of especially small clusters, which may lose one or more molecules while being charged or via possible fragmentation processes inside the instrument (Zhao et al., 2011; Kuerten et al., 2014; Ortega et al., 2014). There are many factors that could affect observations, such as the sensitivity of the instrument (Jen et al., 2015, 2016), the ion-molecule reaction (including proton transfer, ion molecule aggregation, and ion decomposition, et al.) (Tsona et al., 2015), and the reagent ions (acetate or nitrate) used (Kuerten et al., 2018). Specifically, sulfuric acid dimers are likely to lose all base and water molecules upon CI using nitrate (Jen et al., 2014).

3.3. Theoretical calculations: structures and thermodynamic parameters

In this work, the capability of MSA to bind with small, electrically neutral SA clusters in the presence of W was examined by theoretical calculations. We studied the SA-MSA-W molecular clusters and simulation system cover cluster sizes containing up to 3 SA and 3 MSA molecules that were hydrated by 0–3 W molecules. The minimum structures of xMSA-ySA-zW (x, y, z = 0-3) under the DF-LMP2-F12/PVTZ//PW91PW91/6-311 + + G (3df, 3pd) level are presented in Fig. 4 and Fig. S5. So far, the theoretical study of MSA-SA-W ternary system has not been found yet, but the studies of heterodimers (including MSA-SA, SA-W, and MSA-W system) were relatively more (Kreidenweis et al., 1989; Wyslouzil et al., 1991a,b; Arstila et al., 1998; Ball et al., 1999; Noppel et al., 2002; Hanson and Lovejoy, 2006; Brus et al., 2010; Sipila et al., 2010; Dawson et al., 2012; Zollner et al., 2012; Bork et al., 2014b; Jen et al., 2014, 2016; Chen et al., 2015; Glasoe et al., 2015; Olenius et al., 2017). For the dimer and trimer clusters, such as $(SA)_2$, $(MSA)_2$, MSA-SA, $(SA)_3$, $(MSA)_3$, $(SA)_2$-MSA, and SA-$(MSA)_2$, the minimum structures are consistent with the available data in previously studies (Bork et al., 2014b; Chen et al., 2015). However, for the SA-W_3 system, we found a lower energy structure compared to that presented in Laaksonen et al.'s work (Arstila et al., 1998), and applied the newly structure in the subsequent model simulations. Generally, proton transfer phenomenon was observed for all the heteromolecular clusters and the ternary clusters, and the clusters were stabilized by both hydrogen bonds and electrostatic interactions between positive and negative substances.

The electronic energies and thermochemical parameters of the MSA-SA-W systems were first computed with quantum chemical methods. The thermodynamic data for all studied clusters, including the data of the clusters formed by their constituent molecules in the MSA-SA-W system are shown in Table S2 in the SI. The Gibbs free energy calculated for $(SA)_2$, $(MSA)_2$, and SA-MSA clusters in this study was −6.03 kcal/mol, −5.72 kcal/mol, and −6.72 kcal/mol, respectively, under the DF-LMP2-F12/PVTZ//PW91PW91/6-311 + + G(3df, 3pd) level of theory, which are relatively smaller than those reported under the higher CCSD (T)-F12/VDZ-F12// M06-2X/6-311 + + G(3df,3pd) level (Bork et al., 2014a). However, the overall trend of the change is consistent.

Compared to the massive studies of MSA-amines (Napari et al., 2002; Dawson et al., 2014; Chen et al., 2016; Arquero et al., 2017), the calculated enthalpy change (Δ H) and Gibbs free energy change (Δ G) of MSA-SA system is much weaker than the MSA-amines (TMA/DMA/MA)

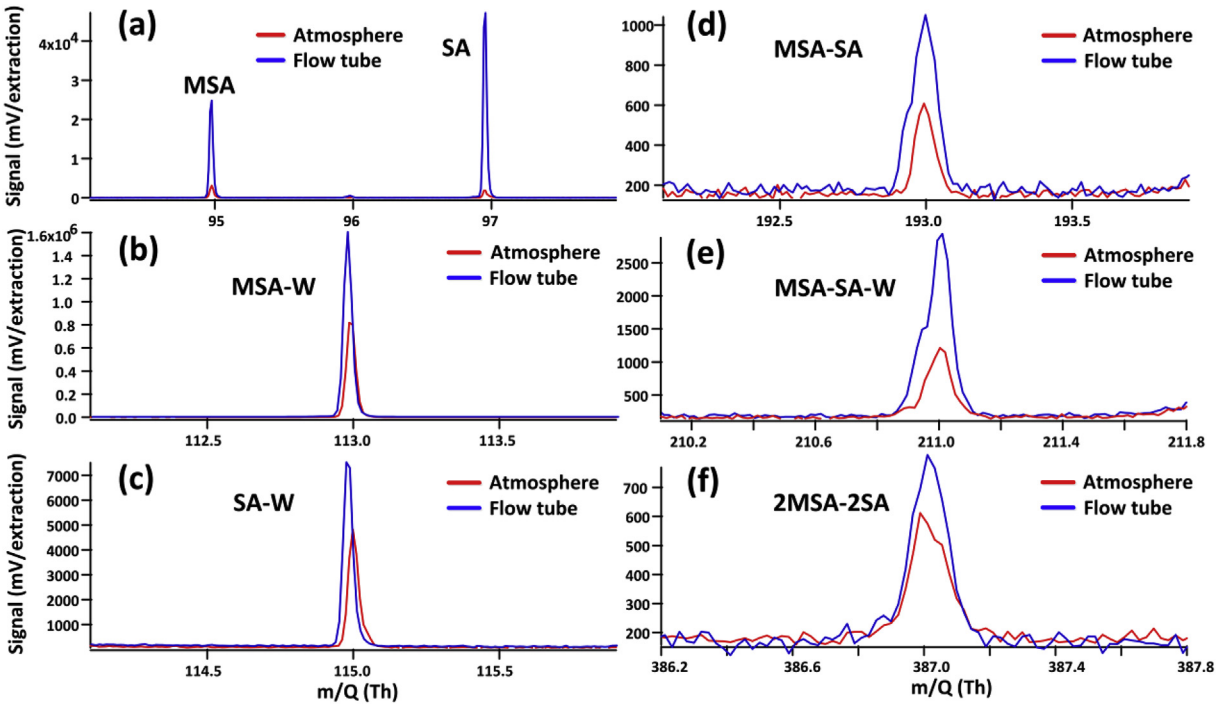

Fig. 3. Selected mass spectra of (a) the bare MSA^- and SA^-, (b) the hydrated MSA ($MSA^-{\cdot}H_2O$) cluster, (c) the hydrated SA ($SA^-{\cdot}H_2O$) cluster, (d) the MSA-SA binary anionic cluster, (e) the MSA-SA-W ternary anionic cluster, and (f) the MSA_2-SA_2 anionic clusters generated in the flow tube reactor (blue peak) measured by the CI-APi-TOF-MS. The red peak in each plot represents the background (i.e., ambient condition) for comparison.

species under the MP2/aug-cc-pV(D + d)z level. This may indicate that the MSA-SA system is not as stable as MSA-bases species. A previous study (Bork et al., 2014b) has investigated the effect and role of MSA in the formation of molecular clusters in atmospheres containing various quantities of MSA, SA and dimethyl amine (DMA), they found that MSA may increase the cluster formation rates of SA-DMA by up to 1 order of magnitude, which is also indicated that the MSA contribute to the NPF event is less.

Since MSA is a weak acid than SA, it is expected that the SA is more efficient than MSA at forming particles with W. It is surprising that the MSA-SA bond is stronger than the SA-SA bond. This may also suggest that the strength of the hydrogen bonding interaction (the extent of the proton-transfer) needed to form an ion pair may also be important. The addition of MSA to the SA-W system can enhance the formation of particles and could be attributed to the following mechanisms: 1) increased chance of hydrogen bonding. The clusters have hydrogen bonding sites that can be used spatially for further addition of substance, leading to cluster growth (Dawson et al., 2012); or 2) the encouragement of proton transfer between the molecules, which could forming the ion pair to facilitate the cluster growth (Li et al., 2007; Weber et al., 2012).

In the formation of MSA-SA-W cluster, the presence of acid dissociation (as one kind of proton-transfer) plays an important role in the stability of the system. Both of these effects may lead to an increase in NPF. By providing a mechanism for attracting and retaining additional acids, bases and water molecules, the presence of hydrogen-bonding sites in small clusters may play a role.

3.4. Modeling simulations

Direct comparisons between theoretical and observed values are not possible solely based on predictions of cluster stabilities: quantum chemical approaches probe the properties of individual clusters, while NPF experiments primarily address cluster concentrations that result from the combination of all dynamic processes involving the clusters and vapor molecules. Thus, connecting predictions with measurable quantities requires modeling a population of clusters that considers collisions, evaporations, vapor sources, the attachment of clusters to surfaces, and possibly other processes depending on the situation (Olenius et al., 2017). Quantum chemistry calculation results can be used in cluster population modeling to obtain cluster evaporation rate constants, which can be obtained from the free energies of formation and collision rate constants.

The cluster populations were modeled in two different situations: a time-dependent situation corresponding to a laminar flow tube experiment, and a time-independent steady-state situation at different vapor concentrations, relative humidities, and temperatures representative of conditions relevant to the atmospheric boundary layer. Quantum chemical data sets of (0-3) MSA, (0-3) SA and (0-3) W clusters were complemented with additional clusters and hydrates, and the quantum chemistry calculation-based evaporation rate values were implemented in a parameter-free dynamics cluster model to study the steady-state of the SA dimer concentration and cluster formation rates under different simulated conditions. With respect to the acid-acid cluster growth, the stability of the cluster can be inferred by comparing the evaporation rate and the collision rate, which largely depends on the collision rate and the concentration of the two acid molecules. However, the collision rate constants of the studied clusters are close to each other, so the difference in evaporation rate can be used to indicate the stability of the clusters at a given acid concentrations. The evaporation rates of xMSA-ySA (x, y = 0-3) at 298.15 K and 30% RH are shown in Table 1.

Generally, the evaporation rates of 3MSA, 3SA-2MSA, and 3SA-1MSA are ranged from 10^{-1} s^{-1} to 10^{-3} s^{-1}, which is lower than those for other studied cluster. In the simulation conditions, where the SA concentration was 4×10^9 cm^{-3} and the MSA concentration was 4.0×10^{10} molecule cm^{-3}, clusters with evaporation rates between 10^{-1} and 10^{-3} s^{-1} can be considered stable, and the 3SA-2MSA formed by the 3SA and 2MSA pathway and the 3SA-1MSA formed by the 3SA and 1MSA pathway are the most stable clusters. By examining all the evaporation pathways, it was found that the evaporation of an SA or an MSA monomer was the main attenuation pathway for all

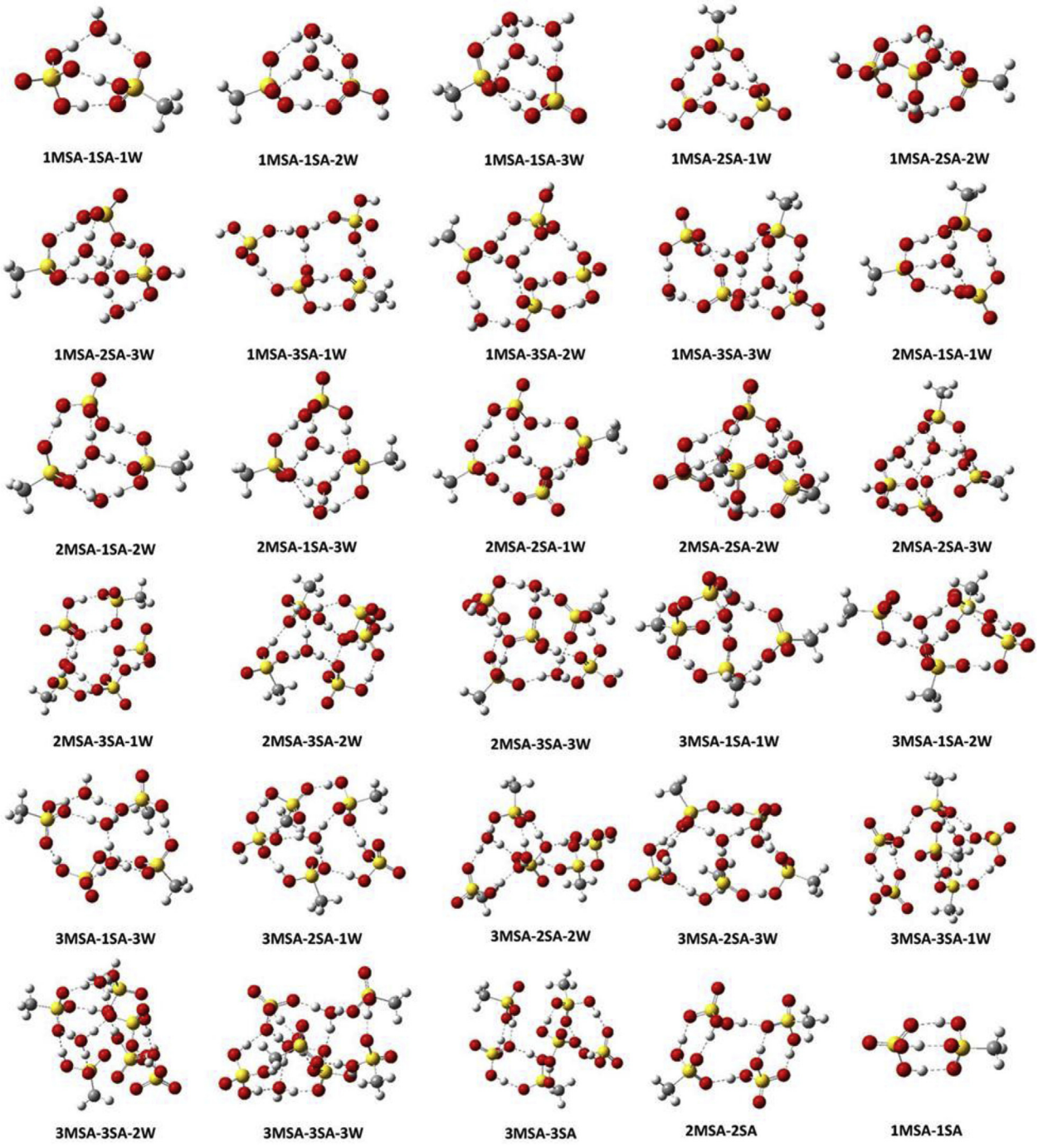

Fig. 4. Minima structures for xMSA-ySA-zW (x, y, z = 0-3) under the DF-LMP2-F12/PVTZ//PW91PW91/6-311 + + G (3df, 3pd) level. Red balls represent oxygen atoms, gray balls represent carbon atoms, yellow balls represent sulfur atoms, and white balls represent hydrogen atoms. (For interpretation of the references to colour in this figure legend, the reader is referred to the Web version of this article.)

studied clusters. It should be noted that the 1SA-1MSA cluster with an evaporation rate of 10^1 s^{-1} was also considered to be stable, which is consistent with the result observed with mass spectrometry.

Cluster growth flux was also shown in Table 1, the negative growth flux indicates that the cluster is not in the equilibrium condition. Take 3SA·2MSA for instance, only 3SA·1MSA + 1MSA path could form 3SA·2MSA, however, 3SA·1MSA cluster has no channel to form. Thus, 3SA·2MSA cluster may not participate in the particle nucleation and further growth. By the similar way, the clusters 2SA·3MSA, 2SA·2MSA, and 1SA·3MSA could contribute the most to the particle formation.

The formation rate of clusters and the SA dimer concentrations can be used as two main quantities to characterize the stabilization potential of a given substance in SA-based NPF (Jen et al., 2014). In the current study, the flux of clusters that grew successfully outside of the 3 × 3 simulation system was recorded as the formation rate (J_{calc}). The cluster population was modeled in a time-dependent situation corresponding to the flow tube reactor. The simulation setup mimicking the conditions of the laminar flow tube was similar to that described above.

Fig. 5 shows the cluster formation rates (J_{calc}) as a function of relative humidity (RH: ranging from 0 to 80%) for an SA concentration of 4.0×10^9 molecule cm^{-3}, an MSA concentration of 4.0×10^{10} molecule cm^{-3}, and a temperature of 298.15 K. Generally, the cluster

Table 1
Evaporation rates and cluster growth flux for SA binding with MSA in the 3×3 size box at 298.15 K, and 30% RH.

Fragment1	Fragment2	Product cluster	Evaporation rate (s^{-1})	Cluster growth Flux (cm^{-3} s^{-1})
2MSA	1MSA	3MSA	8.83e-01	1.80e+16
3MSA	3SA	3SA·3MSA	5.81e+10	−6.83e+05
3SA·2MSA	1MSA	3SA·3MSA	3.94e+13	−4.20e+07
3SA·1MSA	2MSA	3SA·3MSA	2.45e+12	3.97e+07
2SA·3MSA	1SA	3SA·3MSA	7.95e+04	−9.34e-01
2SA·2MSA	1SA·1MSA	3SA·3MSA	1.81e+11	−2.05e+06
2SA·1MSA	1SA·2MSA	3SA·3MSA	1.93e+12	−2.27e+07
2SA	1SA·3MSA	3SA·3MSA	6.04e+00	−7.11e-05
3SA·1MSA	1MSA	3SA·2MSA	2.92e+02	8.14e+08
3SA	2MSA	3SA·2MSA	1.58e-03	−2.13e+04
2SA·2MSA	1SA	3SA·2MSA	1.63e-01	−2.04e+06
2SA·1MSA	1SA·1MSA	3SA·2MSA	2.62e+01	−3.65e+08
2SA	1SA·2MSA	3SA·2MSA	5.38e+01	−7.70e+08
3SA	1MSA	3SA·1MSA	7.55e-03	−1.31e+06
2SA·1MSA	1SA	3SA·1MSA	2.24e+00	−3.68e+08
2SA	1SA·1MSA	3SA·1MSA	1.14e+02	−5.91e+08
2SA	1SA	3SA	1.87e+07	−9.15e+09
1MSA	1MSA	2MSA	8.14e+02	5.27e+17
3MSA	2SA	2SA·3MSA	3.39e+13	−3.38e+10
2MSA	2SA·1MSA	2SA·3MSA	2.33e+09	7.06e+06
2SA·2MSA	1MSA	2SA·3MSA	3.88e+09	−1.09e+06
1SA·3MSA	1SA	2SA·3MSA	9.67e+01	−1.35e-01
1SA·2MSA	1SA·1MSA	2SA·3MSA	1.15e+14	1.89e+10
2MSA	2SA	2SA·2MSA	4.88e+05	−6.41e+10
2SA.·1MSA	1MSA	2SA·2MSA	2.15e+05	−3.45e+10
1SA·2MSA	1SA	2SA·2MSA	4.06e+07	−5.96e+12
1SA·1MSA	1SA·1MSA	2SA·2MSA	1.56e+09	2.08e+14
2SA	1MSA	2SA·1MSA	5.17e+04	−4.57e+11
1SA·1MSA	1SA	2SA·1MSA	6.35e+07	−2.11e+14
1SA	1SA	2SA	6.10e+04	2.57e+15
3MSA	1SA	1SA·3MSA	8.69e+17	−5.21e+14
2MSA	1SA·1MSA	1SA·3MSA	1.32e+15	3.53e+14
1SA·2MSA	1MSA	1SA·3MSA	1.47e+15	7.04e+12
2MSA	1SA	1SA·2MSA	3.13e+04	−1.10e+16
1SA·1MSA	1MSA	1SA·2MSA	4.13e+04	7.90e+15
1MSA	1SA	1SA·1MSA	7.27e+01	3.99e+15

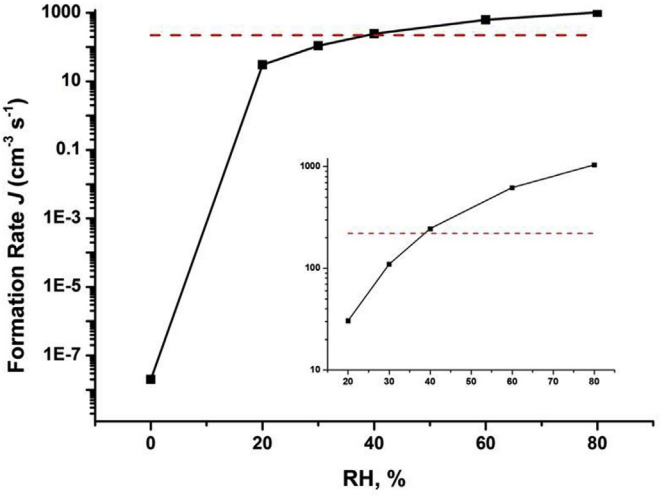

Fig. 5. Simulated formation rates J_{calc} (cm^{-3} s^{-1}) as a function of relative humidity (RH) at 298.15 K, SA concentration (4.0×10^9 molecule cm^{-3}), and MSA concentration (4.0×10^{10} molecule cm^{-3}). The red dashed line represents the result of the *J* value obtained under the experimental conditions (RH: 30%). The inset is a close view of the main figure. (For interpretation of the references to colour in this figure legend, the reader is referred to the Web version of this article.)

formation rate increases with the increasing RH for the considered condition. When the RH < 20%, the simulated cluster formation rate J_{calc} increases rapidly, indicating that the cluster formation was significantly enhanced by the hydration environment, and W plays a key role in the cluster formation. Whereas for the RH > 20%, the J_{calc} increase slowly compared to the RH < 20%, may indicating that 20% RH is the most suitable reaction condition.

It was worth noting that the simulated cluster formation rate J_{calc} was 2.6×10^2 cm^{-3} s^{-1} under RH = 30%, although the value is very close to the data obtained by the experiment ($J_{exp(SA\ -(MSA\text{-}W))}$) = ($1.89 \times 10^2 \pm 36\%$ cm^{-3} s^{-1}), however, there is no comparability between the two values, since a large difference in the size of the selected particles (experiment: > 2.5 nm; theoretical: the maximum size is ~15 Å ≈ 1.5 nm). Thus, more work need to do in the future, such as expand the theoretical simulation size to 4×4×4, even 5×5×5 box to match the experiment conditions. The simulated J_{calc} as a function of the MSA concentration and the SA concentration are also displayed in Figs. S3 and S4 in the SI. In addition, the steady-state SA dimer concentration was approximately 10^4-fold (cm^{-3}) under the same simulated conditions; other steady-state concentrations of each cluster are also shown in Table S3 in the SI.

4. Conclusions

MSA is present in considerable concentrations in the gas phase and aerosols in coastal regions and oceans areas. The potential role of MSA in atmospheric new particle formation (NPF) involving SA and W were explored by experiments and simulations in a range of ambient conditions relevant to the lower troposphere. Flow tube reactor was used to investigate the effects of each reactant on NPF in a multi-component system consisting of MSA, SA, and W. Particles were measured for different combinations of reactants, for typical data for the particle size distribution during the SA-W/MSA-W binary nucleation, and for the ternary system with different adding orders. In the experiment conditions (SA concentration of $4.0 \times 10^9 \pm 35\%$ molecule cm^{-3}, an MSA concentration of $4.0 \times 10^{10} \pm 50\%$ molecule cm^{-3}, an RH of 30 ± 1%, a temperature of 27 ± 1 °C, and a residence time of 28 s), it showed that a different order for reactant addition led to different experimental results, where the added MSA vapor to the SA-W binary system showed an obvious bimodal structure; for ternary system with SA added to the MSA-W, the similar bimodal phenomenon was not observed. This could be due to the different acidity of the two acids.

The composition of clusters in the mixture flow was further analyzed by the CI-APi-TOF-MS. This experimental method resulted in significantly higher concentrations than those commonly found in ambient air; therefore, the improved signal-to-noise ratio enables us to study the reactions between gas-phase species in the ambient air and SA/MSA that contain clusters. Mass peaks corresponding to clusters that contain smaller MSA or SA molecules were clearly observed, indicating that these clusters are stable and exist.

In addition, quantum chemistry data sets of (0-3) MSA, (0-3) SA and (0-3) W clusters were complemented with additional clusters and hydrates, and the quantum chemistry calculation-based evaporation rate values were implemented in a parameter-free dynamics cluster model to study the steady-state of the SA dimer concentration and cluster formation rates under different simulated conditions. The steady state was chosen as a simplified representative situation to examine the effects of different atmospheric conditions. Then proceeded by simulating cluster formation rate populations under a set of conditions relevant to the experiment, where the MSA concentration was generally higher than that in the atmosphere, and the relative humidity covered a range of typical values. We presented and discussed results on SA–MSA clustering in the form of observable quantities.

Our studies indicate that SA could discreetly enhance NPF from the MSA-W system, but MSA has little effect on SA-W in our experimental simulation conditions. MSA, however, is only one of organics found in

air and always coexists with SA; other species might have a greater enhancement effect on NPF. Understanding how acids and W interact at the molecular level in the atmosphere is obviously important for accurately predicting NPF at the regional and global scale.

Acknowledgment

This work was supported by the National Natural Science Foundation of China (Grant No. 41775122, 21403244, 41605099, 41705097, 21573241, 41775112, 41705111, and 41527808), the Key Research Program of Frontier Science, CAS (Grant No. QYZDB-SSW-DQC031), the National Science Fund for Distinguished Young Scholars (Grant No. 41725019), the Key Research Program of Chinese Academy of Sciences (Grant No. ZDRW-ZS-2016-4-3-6),the National Key Research and Development programs (Grant No. 2016YFC0202203 and 2016YFC0202703), and the National Research Program for Key Issues in Air Pollution Control (DQGG0103).

Appendix A. Supplementary data

Supplementary data to this article can be found online at https://doi.org/10.1016/j.atmosenv.2018.11.043.

References

Aalto, P., Hameri, K., Becker, E., Weber, R., Salm, J., Makela, J.M., Hoell, C., O'Dowd, C.D., Karlsson, H., Hansson, H.C., Vakeva, M., Koponen, I.K., Buzorius, G., Kulmala, M., 2001. Physical characterization of aerosol particles during nucleation events. Tellus B 53 (4), 344–358.

Almeida, J., Schobesberger, S., Kuerten, A., Ortega, I.K., Kupiainen-Maatta, O., Praplan, A.P., Adamov, A., Amorim, A., Bianchi, F., Breitenlechner, M., 2013. Molecular understanding of sulphuric acid-amine particle nucleation in the atmosphere. Nature 502 (7471), 359–364.

Arquero, K.D., Gerber, R.B., Finlayson-Pitts, B.J., 2017. The role of oxalic acid in new particle formation from methanesulfonic acid, methylamine, and water. Environ. Sci. Technol. 51 (4), 2124–2130.

Arstila, H., Laasonen, K., Laaksonen, A., 1998. Ab initio study of gas-phase sulphuric acid hydrates containing 1 to 3 water molecules. J. Chem. Phys. 108 (3), 1031–1039.

Ball, S.M., Hanson, D.R., Eisele, F.L., McMurry, P.H., 1999. Laboratory studies of particle nucleation: initial results for H_2SO_4, H_2O, and NH_3 vapors. J. Geophys. Res. Atmos. 104 (D19), 23709–23718.

Barnes, I., Hjorth, J., Mihalopoulos, N., 2006. Dimethyl sulfide and dimethyl sulfoxide and their oxidation in the atmosphere. Chem. Rev. 106 (3), 940–975.

Berresheim, H., Eisele, F.L., Tanner, D.J., McInnes, L.M., Ramseybell, D.C., Covert, D.S., 1993. Atmospheric sulfur chemistry and cloud condensation nuclei (CCN) concentrations over the northeastern parcific coast. J. Geophys. Res. Atmos. 98 (D7), 12701–12711.

Berresheim, H., Elste, T., Tremmel, H.G., Allen, A.G., Hansson, H.C., Rosman, K., Dal Maso, M., Makela, J.M., Kulmala, M., O'Dowd, C.D., 2002. Gas-aerosol relationships of H_2SO_4, MSA, and OH: observations in the coastal marine boundary layer at Mace Head, Ireland. J. Geophy. Res. Atmos. 107 (D19), 8100–8112.

Bianchi, F., Praplan, A.P., Sarnela, N., Dommen, J., Kuerten, A., Ortega, I.K., Schobesberger, S., Junninen, H., Simon, M., Troestl, J., 2014. Insight into acid-base nucleation experiments by comparison of the chemical composition of positive, negative, and neutral clusters. Environ. Sci. Technol. 48 (23), 13675–13684.

Bianchi, F., Trostl, J., Junninen, H., Frege, C., Henne, S., Hoyle, C.R., Molteni, U., Herrmann, E., Adamov, A., Bukowiecki, N., 2016. New particle formation in the free troposphere: a question of chemistry and timing. Science 352 (6289), 1109–1112.

Bork, N., Du, L., Kjaergaard, H.G., 2014a. Identification and characterization of the HCl-DMS gas phase molecular complex via infrared spectroscopy and electronic structure calculations. J. Phys. Chem. A 118 (8), 1384–1389.

Bork, N., Elm, J., Olenius, T., Vehkamaki, H., 2014b. Methane sulfonic acid-enhanced formation of molecular clusters of sulfuric acid and dimethyl amine. Atmos. Chem. Phys. 14 (22), 12023–12030.

Brus, D., Hyvarinen, A.P., Viisanen, Y., Kulmala, M., Lihavainen, H., 2010. Homogeneous nucleation of sulfuric acid and water mixture: experimental setup and first results. Atmos. Chem. Phys. 10 (6), 2631–2641.

Brus, D., Skrabalova, L., Herrmann, E., Olenius, T., Travnickova, T., Makkonen, U., Merikanto, J., 2017. Temperature-dependent diffusion of H_2SO_4 in air at atmospherically relevant conditions: laboratory measurements using laminar flow technique. Atmos. Chem. Phys. 8 (7), 132–147 2017.

Bzdek, B.R., Ridge, D.P., Johnston, M.V., 2011. Reactivity of methanesulfonic acid salt clusters relevant to marine air. J. Geophys. Res. Atmos. 116, D03301–D03308.

Chen, H., Ezell, M.J., Arquero, K.D., Varner, M.E., Dawson, M.L., Gerber, R.B., Finlayson-Pitts, B.J., 2015. New particle formation and growth from methanesulfonic acid, trimethylamine and water. Phys. Chem. Chem. Phys. 17 (20), 13699–13709.

Chen, H., Varner, M.E., Gerber, R.B., Finlayson-Pitts, B.J., 2016. Reactions of methanesulfonic acid with amines and ammonia as a source of new particles in air. J. Phys. Chem. B 120 (8), 1526–1536.

Chen, J., Jiang, S., Liu, Y.R., Huang, T., Wang, C.Y., Miao, S.K., Wang, Z.Q., Zhang, Y., Huang, W., 2017. Interaction of oxalic acid with dimethylamine and its atmospheric implications. RSC Adv. 7 (11), 6374–6388.

Chen, M., Titcombe, M., Jiang, J., Jen, C., Kuang, C., Fischer, M.L., Eisele, F.L., Siepmann, J.I., Hanson, D.R., Zhao, J., 2012. Acid-base chemical reaction model for nucleation rates in the polluted atmospheric boundary layer. Proc. Natl. Acad. Sci. U.S.A. 109 (46), 18713–18718.

Dal Maso, M., Sogacheva, L., Aalto, P.P., Riipinen, I., Komppula, M., Tunved, P., Korhonen, L., Suur-Uski, V., Hirsikko, A., Kurten, T., Kerminen, V.M., Lihavainen, H., Viisanen, Y., Hansson, H.C., Kulmala, M., 2007. Aerosol size distribution measurements at four Nordic field stations: identification, analysis and trajectory analysis of new particle formation bursts. Tellus 59 B, 350–361.

Dall'Osto, M., Ceburnis, D., Monahan, C., Worsnop, D.R., Bialek, J., Kulmala, M., Kurten, T., Ehn, M., Wenger, J., Sodeau, J., 2012. Nitrogenated and aliphatic organic vapors as possible drivers for marine secondary organic aerosol growth. J. Geophys. Res. Atmos. 117, D12311–D12321.

Dawson, M.L., Varner, M.E., Perraud, V., Ezell, M.J., Gerber, R.B., Finlayson-Pitts, B.J., 2012. Simplified mechanism for new particle formation from methanesulfonic acid, amines, and water via experiments and ab initio calculations. Proc. Natl. Acad. Sci. U.S.A. 109 (46), 18719–18724.

Dawson, M.L., Varner, M.E., Perraud, V., Ezell, M.J., Wilson, J., Zelenyuk, A., Gerber, R.B., Finlayson-Pitts, B.J., 2014. Amine-amine exchange in aminium-methanesulfonate aerosols. J. Phys. Chem. C 118 (50), 29431–29440.

Delley, B., 1990. An all-electron numerical method for solving the local density functional for functional for ployatomic molecules. J. Chem. Phys. 92 (1), 508–517.

Donahue, N.M., Ortega, I.K., Chuang, W., Riipinen, I., Riccobono, F., Schobesberger, S., Dommen, J., Baltensperger, U., Kulmala, M., Worsnop, D.R., 2013. How do organic vapors contribute to new-particle formation? Faraday Discuss 165, 91–104.

Ehn, M., Thornton, J.A., Kleist, E., Sipila, M., Junninen, H., Pullinen, I., Springer, M., Rubach, F., Tillmann, R., Lee, B., 2014. A large source of low-volatility secondary organic aerosol. Nature 506 (7489), 476–482.

Eisele, F.L., Tanner, D.J., 1993. Measurement of the gas-phase concentration of H_2SO_4 and methanesulfonic-acid and estimates of H_2SO_4 production and loss in the atmosphere. J. Geophys. Res. Atmos. 98 (D5), 9001–9010.

Elm, J., Myllys, N., Olenius, T., Halonen, R., Kurten, T., Vehkamaki, H., 2017. Formation of atmospheric molecular clusters consisting of sulfuric acid and $C_8H_{12}O_6$ tricarboxylic acid. Phys. Chem. Chem. Phys. 19 (6), 4877–4886.

Erupe, M.E., Viggiano, A.A., Lee, S.H., 2011. The effect of trimethylamine on atmospheric nucleation involving H_2SO_4. Atmos. Chem. Phys. 11 (10), 4767–4775.

Ezell, M.J., Chen, H., Arquero, K.D., Finlayson-Pitts, B.J., 2014. Aerosol fast flow reactor for laboratory studies of new particle formation. J. Aerosol Sci. 78, 30–40.

Ezell, M.J., Johnson, S.N., Yu, Y., Perraud, V., Bruns, E.A., Alexander, M.L., Zelenyuk, A., Dabdub, D., Finlayson-Pitts, B.J., 2010. A new aerosol flow system for photochemical and thermal studies of tropospheric aerosols. Aerosol Sci. Technol. 44 (5), 329–338.

Farmer, D.K., Cappa, C.D., Kreidenweis, S.M., 2015. Atmospheric processes and their controlling influence on cloud condensation nuclei activity. Chem. Rev. 115 (10), 4199–4217.

Frisch, M.J., Schlegel, H.B., Scuseria, G.E., Robb, M.A., Scalmani, G., Barone, V., Mennucci, B., Petersson, G.A., Caricato, M., Li, X., Hratchian, H.P., Izmaylov, A.F., Zheng, G., Sonnenberg, J.L., Hada, M., 2009. Gaussian 09, Revision A.02. Gaussian, Inc., Wallingford CT.

Glasoe, W.A., Volz, K., Panta, B., Freshour, N., Bachman, R., Hanson, D.R., McMurry, P.H., Jen, C., 2015. Sulfuric acid nucleation: an experimental study of the effect of seven bases. J. Geophys. Res. Atmos. 120 (5), 1933–1950.

Hanson, D.R., Lovejoy, E.R., 2006. Measurement of the thermodynamics of the hydrated dimer and trimer of sulfuric acid. J. Phys. Chem. A 110 (31), 9525–9528.

Heal, M.R., Kumar, P., Harrison, R.M., 2012. Particles, air quality, policy and health. Chem. Soc. Rev. 41 (19), 6606–6630.

Henschel, H., Kurten, T., Vehkamaki, H., 2016. Computational study on the effect of hydration on new particle formation in the sulfuric acid/ammonia and sulfuric acid/dimethylamine systems. J. Phys. Chem. A 120 (11), 1886–1896.

Jen, C.N., Hanson, D.R., McMurry, P.H., 2015. Toward reconciling measurements of atmospherically relevant clusters by chemical ionization mass spectrometry and mobility classification/vapor condensation. Aerosol Sci. Technol. 49 (1), I–III.

Jen, C.N., McMurry, P.H., Hanson, D.R., 2014. Stabilization of sulfuric acid dimers by ammonia, methylamine, dimethylamine, and trimethylamine. J. Geophys. Res. Atmos. 119 (12), 7502–7514.

Jen, C.N., Zhao, J., McMurry, P.H., Hanson, D.R., 2016. Chemical ionization of clusters formed from sulfuric acid and dimethylamine or diamines. Atmos. Chem. Phys. 16 (19), 12513–12529.

Jokinen, T., Berndt, T., Makkonen, R., Kerminen, V.M., Junninen, H., Paasonen, P., Stratmann, F., Herrmann, H., Guenther, A.B., Worsnop, D.R., 2015. Production of extremely low volatile organic compounds from biogenic emissions: measured yields and atmospheric implications. Proc. Natl. Acad. Sci. U.S.A. 112 (23), 7123–7128.

Junninen, H., Ehn, M., Petaja, T., Luosujarvi, L., Kotiaho, T., Kostiainen, R., Rohner, U., Gonin, M., Fuhrer, K., Kulmala, M., Worsnop, D.R., 2010. A high-resolution mass spectrometer to measure atmospheric ion composition. Atmos. Meas.Tech. 3 (4), 1039–1053.

Kangasluoma, J., Kuang, C., Wimmer, D., Rissanen, M.P., Lehtipalo, K., Ehn, M., Worsnop, D.R., Wang, J., Kulmala, M., Petaja, T., 2014. Sub-3 nm particle size and composition dependent response of a nano-CPC battery. Atmos. Meas. Tech. 7 (3), 689–700.

Kerminen, V.M., Lihavainen, H., Komppula, M., Viisanen, Y., Kulmala, M., 2005. Direct observational evidence linking atmospheric aerosol formation and cloud droplet activation. Geophys. Res. Lett. 32 (14), L14803–L14807.

Kirkby, J., Curtius, J., Almeida, J., Dunne, E., Duplissy, J., Ehrhart, S., Franchin, A., Gagne, S., Ickes, L., Kuerten, A., 2011. Role of sulphuric acid, ammonia and galactic cosmic rays in atmospheric aerosol nucleation. Nature 476 (7361), 429–477.
Korhonen, P., Kulmala, M., Laaksonen, A., Viisanen, Y., McGraw, R., Seinfeld, J.H., 1999. Ternary nucleation of H_2SO_4, NH_3, and H_2O in the atmosphere. J. Geophys. Res. Atmos. 104 (D21), 26349–26353.
Kreidenweis, S.M., Flagan, R.C., Seinfeld, J.H., Okuyama, K., 1989. Binary nucleation of methanesulfonic-acid and water. J. Aerosol Sci. 20 (5), 585–607.
Kuang, C., McMurry, P.H., McCormick, A.V., Eisele, F.L., 2008. Dependence of nucleation rates on sulfuric acid vapor concentration in diverse atmospheric locations. J. Geophys. Res. Atmos. 113 (D10), D10209–D10216.
Kuang, C., Riipinen, I., Sihto, S.L., Kulmala, M., McCormick, A.V., McMurry, P.H., 2010. An improved criterion for new particle formation in diverse atmospheric environments. Atmos. Chem. Phys. 10 (17), 8469–8480.
Kuerten, A., Jokinen, T., Simon, M., Sipila, M., Sarnela, N., Junninen, H., Adamov, A., Almeida, J., Amorim, A., Bianchi, F., 2014. Neutral molecular cluster formation of sulfuric acid-dimethylamine observed in real time under atmospheric conditions. Proc. Natl. Acad. Sci. U.S.A. 111 (42), 15019–15024.
Kuerten, A., Li, C., Bianchi, F., Curtius, J., Dias, A., Donahue, N.M., Duplissy, J., Flagan, R.C., Hakala, J., Jokinen, T., 2018. New particle formation in the sulfuric acid-dimethylamine-water system: reevaluation of CLOUD chamber measurements and comparison to an aerosol nucleation and growth model. Atmos. Chem. Phys. 18 (2), 845–863.
Kulmala, M., Kerminen, V.M., 2008. On the formation and growth of atmospheric nanoparticles. Atmos. Res. 90 (2–4), 132–150.
Kulmala, M., Vehkamaki, H., Petaja, T., Dal Maso, M., Lauri, A., Kerminen, V.M., Birmili, W., McMurry, P.H., 2004. Formation and growth rates of ultrafine atmospheric particles: a review of observations. J. Aerosol Sci. 35 (2), 143–176.
Kurten, T., Loukonen, V., Vehkamaki, H., Kulmala, M., 2008. Amines are likely to enhance neutral and ion-induced sulfuric acid-water nucleation in the atmosphere more effectively than ammonia. Atmos. Chem. Phys. 8 (14), 4095–4103.
Li, S., Zhang, L., Qin, W., Tao, F.M., 2007. Intermolecular structure and properties of the methanesulfonic acid-ammonia system in small water clusters. Chem. Phys. Lett. 447 (1–3), 33–38.
Liu, Y.R., Wen, H., Huang, T., Lin, X.X., Gai, Y.B., Hu, C.J., Zhang, W.J., Huang, W., 2014. Structural exploration of water, nitrate/water, and oxalate/water clusters with Basin-hopping method using a compressed sampling technique. J. Phys. Chem. A 118 (2), 508–516.
Mauldin, R.L., Cantrell, C.A., Zondlo, M.A., Kosciuch, E., Ridley, B.A., Weber, R., Eisele, F.E., 2003. Measurements of OH, H_2SO_4, and MSA during tropospheric ozone production about the spring equinox (TOPSE). J. Geophys. Res. Atmos. 108 (D4), 8366–8380.
Mauldin, R.L., Tanner, D.J., Heath, J.A., Huebert, B.J., Eisele, F.L., 1999. Observations of H_2SO_4 and MSA during PEM-tropics-A. J. Geophys. Res. Atmos. 104 (D5), 5801–5816.
McGrath, M.J., Olenius, T., Ortega, I.K., Loukonen, V., Paasonen, P., Kurten, T., Kulmala, M., Vehkamaki, H., 2012. Atmospheric Cluster Dynamics Code: a flexible method for solution of the birth-death equations. Atmos. Chem. Phys. 12 (5), 2345–2355.
Meinardi, S., Simpson, I.J., Blake, N.J., Blake, D.R., Rowland, F.S., 2003. Dimethyl disulfide (DMDS) and dimethyl sulfide (DMS) emissions from biomass burning in Australia. Geophys. Res. Lett. 30 (9), 1454–1461.
Nadykto, A.B., Herb, J., Yu, F., Xu, Y., Nazarenko, E.S., 2015. Estimating the lower limit of the impact of amines on nucleation in the earth's atmosphere. Entropy 17 (5), 2764–2780.
Nadykto, A.B., Yu, F., 2007. Strong hydrogen bonding between atmospheric nucleation precursors and common organics. Chem. Phys. Lett. 435 (1–3), 14–18.
Napari, I., Kulmala, M., Vehkamaki, H., 2002. Ternary nucleation of inorganic acids, ammonia, and water. J. Chem. Phys. 117 (18), 8418–8425.
Nishino, N., Arquero, K.D., Dawson, M.L., Finlayson-Pitts, B.J., 2014. Infrared studies of the reaction of methanesulfonic acid with trimethylamine on surfaces. Environ. Sci. Technol. 48 (1), 323–330.
Noppel, M., Vehkamaki, H., Kulmala, M., 2002. An improved model for hydrate formation in sulfuric acid-water nucleation. J. Chem. Phys. 116 (1), 218–228.
O'Dowd, C., McFiggans, G., Creasey, D.J., Pirjola, L., Hoell, C., Smith, M.H., Allan, B.J., Plane, J.M.C., Heard, D.E., Lee, J.D., 1999. On the photochemical production of new particles in the coastal boundary layer. Geophys. Res. Lett. 26 (12), 1707–1710.
Olenius, T., Halonen, R., Kurten, T., Henschel, H., Kupiainen-Maata, O., Ortega, I.K., Jen, C.N., Vehkamaki, H., Riipinen, I., 2017. New particle formation from sulfuric acid and amines: comparison of monomethylamine, dimethylamine, and trimethylamine. J. Geophys. Res. Atmos. 122 (13), 7103–7118.
Ortega, I.K., Olenius, T., Kupiainen-Maatta, O., Loukonen, V., Kurten, T., Vehkamaki, H., 2014. Electrical charging changes the composition of sulfuric acid-ammonia/dimethylamine clusters. Atmos. Chem. Phys. 14 (15), 7995–8007.
Paasonen, P., Nieminen, T., Asmi, E., Manninen, H.E., Petaja, T., Plass-Duelmer, C., Flentje, H., Birmili, W., Wiedensohler, A., Horrak, U., 2010. On the roles of sulphuric acid and low-volatility organic vapours in the initial steps of atmospheric new particle formation. Atmos. Chem. Phys. 10 (22), 11223–11242.
Panta, B., Glasoe, W.A., Zollner, J.H., Carlson, K.K., Hanson, D.R., 2012. Computational fluid dynamics of a cylindrical nucleation flow reactor with detailed cluster thermodynamics. J. Phys. Chem. A 116 (41), 10122–10134.
Peng, X.Q., Huang, T., Miao, S.K., Chen, J., Wen, H., Feng, Y.J., Hong, Y., Wang, C.Y., Huang, W., 2016. Hydration of oxalic acid-ammonia complex: atmospheric implication and Rayleigh-scattering properties. RSC Adv. 6 (52), 46582–46593.
Perdew, J.P., Burke, K., Ernzerhof, M., 1996a. Generalized gradient approximation made simple. Phys. Rev. Lett. 77 (18), 3865–3868.
Perdew, J.P., Burke, K., Wang, Y., 1996b. Generalized gradient approximation for the exchange-correlation hole of a many-electron system. Phys. Rev. B 54 (23), 16533–16539.
Poschl, U., 2005. Atmospheric aerosols: composition, transformation, climate and health effects. Angew. Chem. Int. Ed. 44 (46), 7520–7540.
Raghavachari, K., Trucks, G.W., 1989. Highly correkated system-excitation- energies of 1st row tansition-metals Sc-Cu. J. Chem. Phys. 91 (2), 1062–1065.
Riccobono, F., Schobesberger, S., Scott, C.E., Dommen, J., Ortega, I.K., Rondo, L., Almeida, J., Amorim, A., Bianchi, F., Breitenlechner, M., 2014. Oxidation products of biogenic emissions contribute to nucleation of atmospheric particles. Science 344 (6185), 717–721.
Rosenfeld, P.E., Henry, C.L., Dills, R.L., Harrison, R.B., 2001. Comparison of odor emissions from three different biosolids applied to forest soil. Water, Air, Soil Pollut. 127 (1–4), 173–191.
Schobesberger, S., Junninen, H., Bianchi, F., Lonn, G., Ehn, M., Lehtipalo, K., Dommen, J., Ehrhart, S., Ortega, I.K., Franchin, A., 2013. Molecular understanding of atmospheric particle formation from sulfuric acid and large oxidized organic molecules. Proc. Natl. Acad. Sci. U.S.A. 110 (43), 17223–17228.
Sipila, M., Berndt, T., Petaja, T., Brus, D., Vanhanen, J., Stratmann, F., Patokoski, J., Mauldin, R.L., Hyvarinen, A.P., Lihavainen, H., 2010. The role of sulfuric acid in atmospheric nucleation. Science 327 (5970), 1243–1246.
Spracklen, D.V., Carslaw, K.S., Kulmala, M., Kerminen, V.M., Sihto, S.L., Riipinen, I., Merikanto, J., Mann, G.W., Chipperfield, M.P., Wiedensohler, A., 2008. Contribution of particle formation to global cloud condensation nuclei concentrations. Geophys. Res. Lett. 35 (6), L06808–L06813.
Troestl, J., Chuang, W.K., Gordon, H., Heinritzi, M., Yan, C., Molteni, U., Ahlm, L., Frege, C., Bianchi, F., Wagner, R., 2016. The role of low-volatility organic compounds in initial particle growth in the atmosphere. Nature 533 (7604), 527–535.
Tsona, N.T., Henschel, H., Bork, N., Loukonen, V., Vehkamaki, H., 2015. Structures, hydration, and electrical mobilities of bisulfate ion-sulfuric acid-ammonia/dimethylamine clusters: a computational study. J. Phys. Chem. A 119 (37), 9670–9679.
Vandergheynst, J.S., Cogan, D.J., Defelice, P.J., Gossett, J.M., Walker, L.P., 1998. Effect of process management on the emission of organosulfur compounds and gaseous antecedents from composting processes. Environ. Sci. Technol. 32 (23), 3713–3718.
Vandingenen, R., Raes, F., 1993. Ternary nucleation of methanesulfonic-acid, sulfuric-acid and water vapor. J. Aerosol Sci. 24 (1), 1–17.
Weber, K.H., Morales, F.J., Tao, F.M., 2012. Theoretical study on the structure and stabilities of molecular clusters of oxalic acid with water. J. Phys. Chem. A 116 (47), 11601–11617.
Weber, R.J., Chen, G., Davis, D.D., Mauldin, R.L., Tanner, D.J., Eisele, F.L., Clarke, A.D., Thornton, D.C., Bandy, A.R., 2001. Measurements of enhanced H_2SO_4 and 3-4 nm particles near a frontal cloud during the First Aerosol Characterization Experiment (ACE 1). J. Geophys. Res. Atmos. 106 (D20), 24107–24117.
Weber, R.J., Marti, J.J., McMurry, P.H., Eisele, F.L., Tanner, D.J., Jefferson, A., 1996. Measured atmospheric new particle formation rates: implications for nucleation mechanisms. Chem. Eng. Commun. 151, 53–64.
Weber, R.J., Marti, J.J., McMurry, P.H., Eisele, F.L., Tanner, D.J., Jefferson, A., 1997. Measurements of new particle formation and ultrafine particle growth rates at a clean continental site. J. Geophys. Res. Atmos. 102 (D4), 4375–4385.
Wen, H., Hou, G.L., Liu, Y.R., Wang, X.B., Huang, W., 2016. Examining the structural evolution of bicarbonate-water clusters: insights from photoelectron spectroscopy, basin-hopping structural search, and comparison with available IR spectral studies. Phys. Chem. Chem. Phys. 18 (26), 17470–17482.
Wen, H., Liu, Y.R., Huang, T., Xu, K.M., Zhang, W.J., Huang, W., Wang, L.S., 2013. Observation of linear to planar structural transition in sulfur-doped gold clusters: Au_xS^- (x = 2-5). J. Chem. Phys. 138 (17), 174303–174312.
Wen, H., Liu, Y.R., Xu, K.M., Huang, T., Hu, C.J., Zhang, W.J., Huang, W., 2014. Probing the 2D-to-3D structural transition in gold clusters with a single sulfur atom: $Au_xS^{0,+/-1}$ (x = 1-10). RSC Adv. 4 (29), 15066–15076.
Werner, H.J., Knowles, P.J., Knizia, G., Manby, F.R., Schuetz, M., 2012. Molpro: a general-purpose quantum chemistry program package. WIRES-Comput. Mol. Sci. 2 (2), 242–253.
Werner, H.J., Knizia, G., Manby, F.R., Schuetz, M., 2010. Molpro, Version 2010.1, a Package of Ab Initio Program.
Wyslouzil, B.E., Seinfeld, J.H., Flagan, R.C., Okuyama, K., 1991a. Binary nucleation in acid water-system. 1. Methanesulfonic-acid water. J. Chem. Phys. 94 (10), 6827–6841.
Wyslouzil, B.E., Seinfeld, J.H., Flagan, R.C., Okuyama, K., 1991b. Binary nucleation in acid water-system. 2. Sulfuric-acid water and a comparison with methanesulfonic-acid water. J. Chem. Phys. 94 (10), 6842–6850.
Xu, K.M., Huang, T., Wen, H., Liu, Y.R., Gai, Y.B., Zhang, W.J., Huang, W., 2013. A density functional study of phosphorus-doped gold clusters: Au_nP^- (n = 1-8). RSC Adv. 3 (46), 24492–24502.
Xu, W., Zhang, R., 2012. Theoretical investigation of interaction of dicarboxylic acids with common aerosol nucleation precursors. J. Phys. Chem. A 116 (18), 4539–4550.
Xu, Y., Nadykto, A.B., Yu, F., Jiang, L., Wang, W., 2010. Formation and properties of hydrogen-bonded complexes of common organic oxalic acid with atmospheric nucleation precursors. J. Mol. Struc-Theochem 951 (1–3), 28–33.
Yan, L.L., Liu, Y.R., Huang, T., Jiang, S., Wen, H., Gai, Y.B., Zhang, W.J., Huang, W., 2013. Structure, stability, and electronic property of carbon-doped gold clusters Au_nC^- (n = 1-10): a density functional theory study. J. Chem. Phys. 139 (24), 244312–244325.
Yu, H., McGraw, R., Lee, S.H., 2012. Effects of amines on formation of sub-3 nm particles and their subsequent growth. Geophys. Res. Lett. 39, L02807–L02812.
Zhang, R.Y., Khalizov, A., Wang, L., Hu, M., Xu, W., 2012. Nucleation and growth of nanoparticles in the atmosphere. Chem. Rev. 112 (3), 1957–2011.
Zhang, R.Y., Suh, I., Zhao, J., Zhang, D., Fortner, E.C., Tie, X.X., Molina, L.T., Molina,

M.J., 2004. Atmospheric new particle formation enhanced by organic acids. Science 304 (5676), 1487–1490.
Zhao, J., Smith, J.N., Eisele, F.L., Chen, M., Kuang, C., McMurry, P.H., 2011. Observation of neutral sulfuric acid-amine containing clusters in laboratory and ambient measurements. Atmos. Chem. Phys. 11 (21), 10823–10836.
Zheng, J., Khalizov, A., Wang, L., Zhang, R., 2010. Atmospheric pressure-ion drift chemical ionization mass spectrometry for detection of trace gas species. Anal. Chem. 82 (17), 7302–7308.
Zheng, J., Yang, D., Ma, Y., Chen, M., Cheng, J., Li, S., Wang, M., 2015. Development of a new corona discharge based ion source for high resolution time-of-flight chemical ionization mass spectrometer to measure gaseous H2SO4 and aerosol sulfate. Atmos. Environ. 119, 167–173.
Zollner, J.H., Glasoe, W.A., Panta, B., Carlson, K.K., McMurry, P.H., Hanson, D.R., 2012. Sulfuric acid nucleation: power dependencies, variation with relative humidity, and effect of bases. Atmos. Chem. Phys. 12 (10), 4399–4411.